Spin-polarized photoemission

CY653
Electron Spectroscopy

Akshaya Kumar Samal
CY05D039

Habeeb Muhammed M A
CY05D021

Spin-polarized photoemission

Introduction:

One of the most widely used methods to probe surfaces is by analyzing the energy of the photoemitted electron. The 1905 landmark paper of Einstein, presented the following equation :-

$$E_{kin} = \hbar\omega - \phi - E_i$$

With the advancement in technologies, magnetic materials began to gain prominence in view of their applications in data storage. Thus, the inherent spin-orbit coupling phenomenon is these materials had to be probed and a modified form of photoelectron spectroscopy, where the spin of the ejected electron could be probed was developed. Spin polarized photoelectron yields new and in some cases unique information on the electronic structure of solids and surfaces.

Direction of the spin of photoemitted electrons gives information about photo excitation process and properties of samples.

Two modes to produce a spin polarization of the photoemitted electron.

1. Unpolarized light – excite polarized electrons- magnetic materials- exchange interactions
2. Circularly polarized light-excite transitions between states that are split by spin-orbit interactions- non-magnetic materials

In conventional collision experiments the spin-dependent interactions, such as spin-orbit and exchange interaction, are masked by the much stronger Coulomb interaction. By applying polarized-electron techniques their exploration by specific experiments has now become possible.

The photoexcitation process:

Photoemission represents the excitation of an electron from an initial state, below the Fermi level in the case of condensed matter systems, to a final state above the vacuum level. The initial state may fall within the delocalized valence bands or it may represent a more localized core level. In general, it describes the interaction between the electron and the photon written within the framework of the non-relativistic Schrodinger equation. In such a picture the interaction is accounted for simply by replacing the momentum operator in the Hamiltonian p by p – (e/c) A with $A=A_0\, e^{iwt}$ the vector potential of the electromagnetic field. In doing so this also introduces a term that reflects the scalar potential of the electromagnetic potential Φ. However, it is always possible to chose a gauge such that the latter is zero.

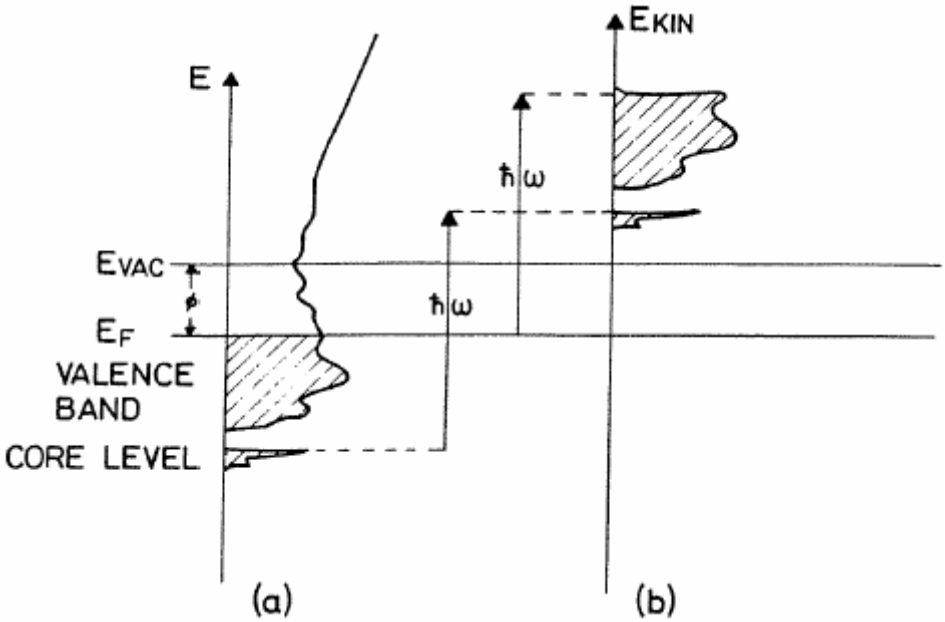

Fig.1. A schematic of the photoemission process. The incident photon with energy $h\omega$ excites an electron from an initial state below the Fermi level E_F to some final state above the vacuum level Evac. The left panel shows the electron originating either from the valence band or the more localized core level. The right panel displays the excited electron energy distribution in the final state.

In studying these systems, the Dirac equation gains prominence since it considers the spin of the electron. The Hamiltonian is suitably modified as

$$H = \frac{1}{2m}\left(p - \frac{e}{c}\boldsymbol{A}\right)^2 + e\phi - \frac{e\bar{h}}{2mc}\boldsymbol{\sigma}\nabla \times \boldsymbol{A} + \frac{ie\bar{h}}{4m^2c^2}\boldsymbol{E}\cdot p - \frac{e\bar{h}}{4m^2c^2}\boldsymbol{\sigma}(\boldsymbol{E}\times p)$$

Where the first two terms are identical to the Schrodinger approach. The third term,proportional to $\sigma\nabla \times A = \sigma .B$ with σ the spin of the electron, represents the interaction of the magnetic dipole with the magnetic field. The fourth term is a relativistic correction to the energy and the final term, proportional to $\sigma(E \times p)$ represents the spin–orbit coupling. The spin-dependent terms in the Dirac equation provide new avenues for inducing spin-polarization effects in the photoemitted beam. The $\sigma .B$ term leads to spin-flip transitions which can lead to a measurable spin-polarization at high photon energies. However, at photon energies typical of the ultraviolet (UV) and soft x-ray range, the probability of spin-flip to spin-conserving transitions is of the order 2×10^{-2}.The spin–orbit term, $\sigma(E \times p)$ can lead to observable spin-polarization effects both in the initial and final states.

Experimental Approaches

1. Spin polarimetry

Much of the pioneering work in spin-polarized photoemission was carried out with spin polarimeters of the high-energy Mott-scattering type. The electrons to be analysed are scattered off gold atoms at energies typically of the order of 100 keV. Spin–orbit coupling of the electron in the potential of the gold atom, as shown in figure 2, leads to an asymmetry in the scattering, left and right, dependent on the spin of the electron.

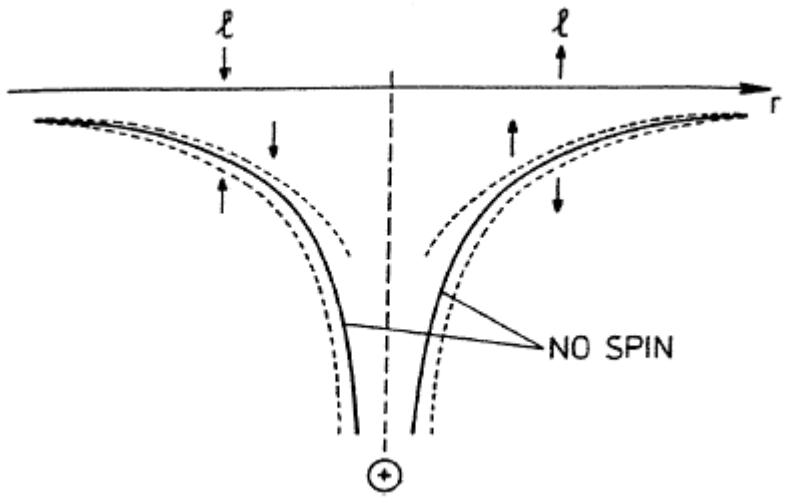

Fig.2 The potential curves experienced by an electron with spin up or spin down in the vicinity of a gold scattering atom both with (- - - -) and without (——) spin–orbit coupling.

Because of the high energies involved in the earlier designs, Mott polarimeters tended to be large. However, there have recently been a number of successful modifications that have allowed the polarimeter to be scaled down in size. After initially passing through a deceleration lens the incident beam of electrons is accelerated onto the gold foil at an energy of 20 keV. Those electrons elastically scattered through 120^0 are detected by two symmetrically opposite channeltrons. Retarding fields in front of the latter collectors remove any electrons that have undergone inelastic losses. The spin polarization *P* of the incident electron beam is given by

$$P = \frac{1}{S}\frac{I_A - I_B}{I_A + I_B}$$

where *S* is called Sherman function of the device, is a measure of its ability to distinguish different spins and *IA* and *IB* represent the intensities measured in opposite channels. Mott polarimeters of this type are now sufficiently small that they can readily be moved inside a vacuum system and, therefore, be used for angle-resolved polarization measurements. The figure of merit (FOM) used in comparing different polarimeters is defined as

$$\mathbf{FOM=S^2\ (I/I_0\ )}$$

where again *S* is the Sherman function, *I* is the sum of the current collected by the two opposite detectors and I_0 is the incident beam current .

Apparatus for spin-polarized photoemission

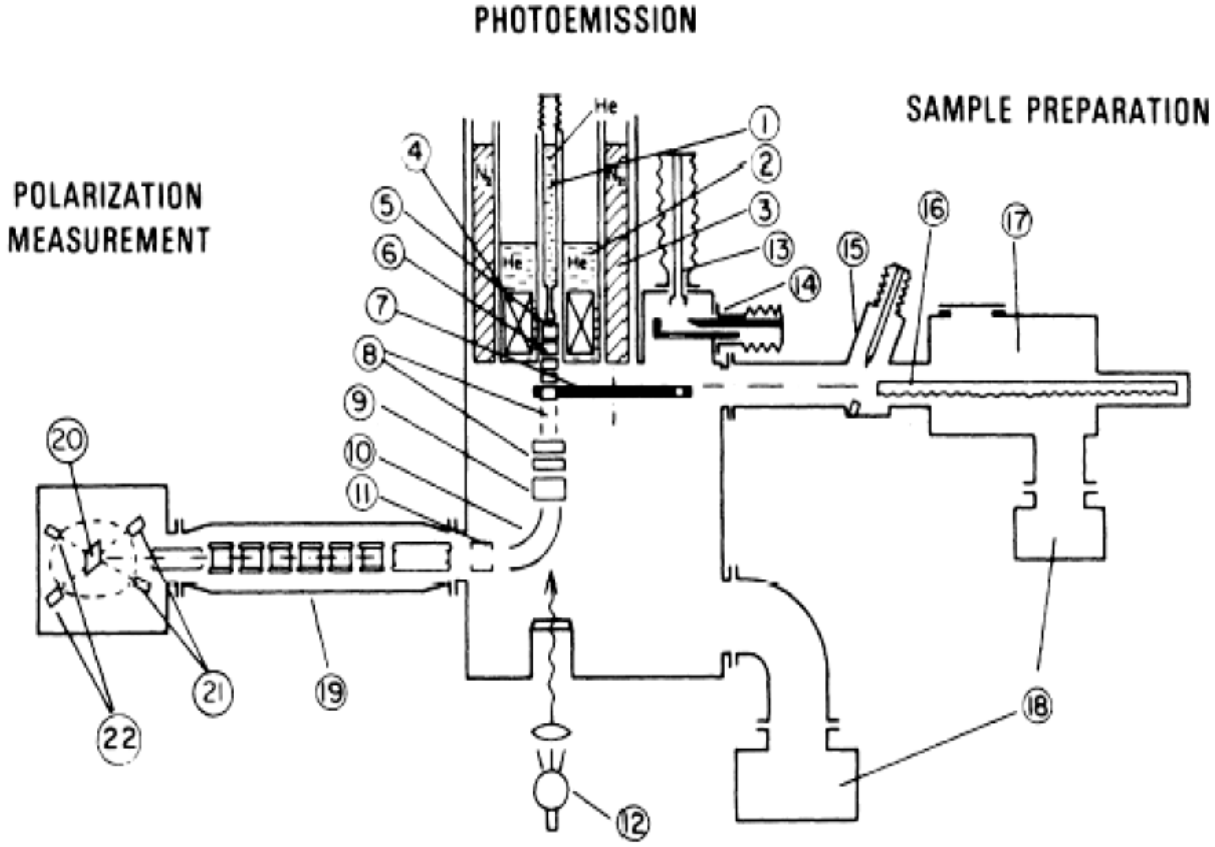

Fig.3 Apparatus for spin-polarized photoemission. 1,gripper with inner cryostat; 2,He cryostat; 3, liquid nitrogen; 4,superconducting coil; 5,sample in measuring position; 6,accelerating electrodes; 7,rotable wheel with samples; 8,parallel beam shifters; 9,plane condenser;10,cylindrical condenser; 11,aperature;12,light source; 13,gripper for cleaving; 14,cleaving mechanism; 15,ultra high vaccum; 16,rack-and-pinion linear motion; 17,sample preparation chamber; 18,ion-getter pumps; 19,seven stage accelerator; 20,gold foil; 21,detector; 22,forward detector to moniter beam

The instrument consists of mainly three parts, namely the photoemission part in the middle , the ESP detection part to the left and the sample preparation part to the right. During the ESP measurement, the sample is attached to the sample holder, which can be maintained at temperature $10K \leq T \leq 600K$.The magnetic field H,up to 50 kOe, is produced by a superconducting coil. The light beam is incident normal to the photoemitting surface .The light source may be a Hg-Xe high pressure arc or a hydrogen discharge monochromatized by a UV spectrograph. The optical system ,with a pressure of 10^{-5} – 10^{-6} Torr, is isolated by a LiF window from the measuring chamber which is maintained at ultra high vacuum conditions.
The electrons photoemitted from the crystal are electrostatically parallel to the magnetic field.The voltage on the rings is adjusted to maximize the intensity of the beam. At an energy of 4.5 keV, the electron beam passes through a series of deflector plates that allow correction of the angle and beam position. The cylindrical deflector deflects the beam by 90^0.Apart from its main function of transforming the longitudional ESP into a transverse one it also deflects the electron beam out of the light beam and discriminates between photoelectrons produced at the acceleration stages by stray light. For the last function, the aperature is essential, since it stops spurious electron from entering the six stage 100 keV electrostatic accelerator. Other aperature at the end of the accelerator define the angle and point of incidence of the electron beam on the Au foil scattering target. The horizontal component of the earth's magnetic field is compensated by a coil.
In the photoemission and electron beam formation section, a pressure of 2×10^{-10} Torr is maintained by an ion getter pump and by the pumping action of the walls of the liquid He cryostat .The sample preparation chamber is connected by an interlock to the measuring chamber. A pressure of 10^{-10} Torr in the sample preparation chamber is maintained by a Ti sublimation pump and by a breakable turbomolecular pump. This chamber contains: (a)an argon ion gun for sputtering of surfaces; (b) a caesium oven for lowering the work function; (c) a mass spectrometer; (d) an electron gun for heating; and (e)a LEED-Auger unit for monitering the state of the surface. The crystal under investigation is positioned on a cog rail and can thus be transported to all the different stages.

2. Spin polarimetry via the exchange interaction:

Spin polarimeters based on an exchange interaction fall into two categories, one is reflection and other is transmission.The scattering surface is a 400 °A thick Fe(001) film grown on an Ag(001) substrate. Reflected intensities are measured when the electrons to be analysed are incident on a magnetized iron surface at an energy of approximately 10 eV.

The asymmetry in the scattering, *A*, in such a detector is given by

$$A = \frac{1}{P}\frac{I^{\uparrow\uparrow} - I^{\uparrow\downarrow}}{I^{\uparrow\uparrow} + I^{\uparrow\downarrow}}$$

where *P* is the spin polarization in the incident beam and $I^{\uparrow\uparrow}$ and $I^{\uparrow\downarrow}$are the scattered intensities obtained when the target and primary beam magnetic moments are parallel and anti-parallel, respectively.
The FOM is given by

$$\mathrm{FOM} = A^2 \frac{I_\mathrm{R}}{I_\mathrm{P}}$$

where I_R and I_P are the reflected and primary beam currents, respectively

In another study in which the spin-dependent electron scattering in ferromagnetic Co films deposited on a Cu(111) substrate. asymmetry in the mean free paths, $\lambda^{\uparrow\downarrow}$ for the two spin states. Measuring the asymmetry

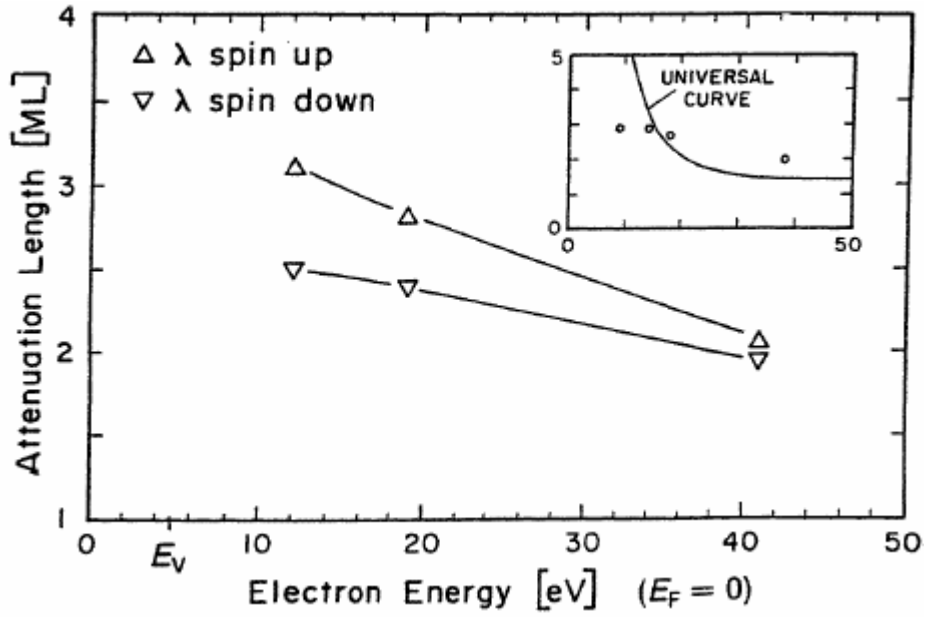

Fig.4 Spin-dependent inelastic mean free paths (IMFP) determined from the spin-polarized photoemission spectra. Values of the spin-averaged IMFP compared to the 'universal' mean free path curve. The electron energies are referenced to the Fermi energy. The error bars on the spin-averaged data reflect the error in the thickness calibration whereas the error bars in the spin-resolved data include only contributions from the polarization uncertainty.

A_λ is defined as

$$A_\lambda = \frac{(\lambda^\uparrow - \lambda^\downarrow)}{(\lambda^\uparrow + \lambda^\downarrow)}$$

as a function of transmission energy they reported a monotonic decrease as the energy increased until at energies above 30 eV it was unclear if any asymmetry existed at all

Practical Applications:

1. Bulk Studies:

Magnetic materials provide an avenue for in-depth study of spin-polarised photoemission, where the incident circularly polarized light can be used to probe spin-orbit interactions. Accordingly, Fig.5 shows the schematic density of states of ferromagnetic Ni. The spin-up and spin-down bands are shifted with respect to one another by the exchange splitting ΔE_{ex} ,which has a theoretical value of ΔE_{ex} = 0.6 eV. But the experimentally obtained value is ~0.3 eV. The exchange splitting is actually energy and wave vector dependant, but the essence of the band magnetism is contained in the figure.

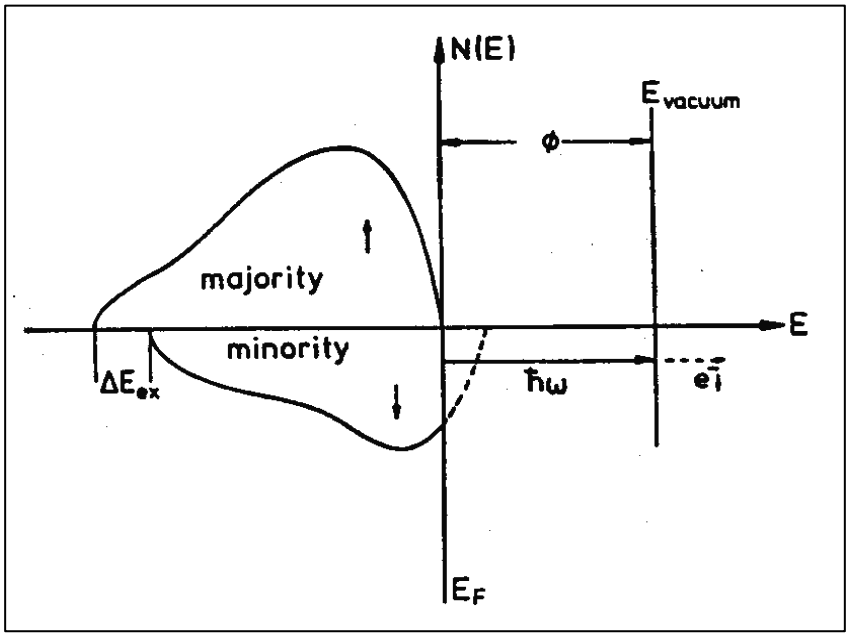

Fig. 5 Photoemission just above the threshold ($\hbar\omega \approx \Phi$) for Ni.Under these conditions only minority spin (spin down) photoelectrons,$e^-_{\downarrow}$, can be observed.

Recent studies on Ni showed that negative photo-ESP can be detected right at threshold, if a single-crystal surface is used instead of a polycrystalline film. To verify this, a (100) surface was prepared by a argon sputtering and annealing the single crystal. The crystallinity and purity of the surface was monitored using Auger spectroscopy, and Low Energy Electron Diffraction. Fig.6 shows the average spectrum of spin polarization obtained from three different experiments on Ni(100). Negative ESP is observed close to threshold, but a steep rise occurs to high positive values of P for photon energies only 50 meV above threshold. P reaches constant value at 8 eV $\leq \hbar\omega \leq$ 9 eV and decay to the model-independent average bulk value of 5% for $\hbar\omega$ > 10 eV within the accuracy of the measurement. The result P = -30% for $\hbar\omega \approx \Phi$ should be taken reservation.

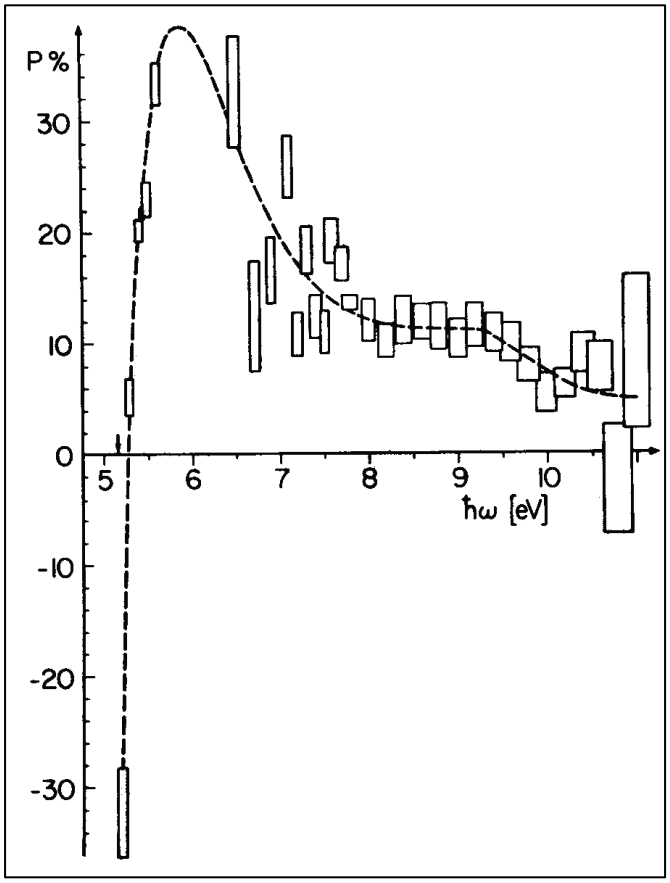

Fig.6 Dependence of photo-ESP on photon energy for a (100) Ni surface at T = 273 K,B=3.4 kG. Photothreshold is indicated by narrow.

Right at threshold it will be mainly steps and other irregular points of the surface that make up the photocurrent. However, all the surfaces consistently showed negative ESP, and the main emphasis lies in the sign of the ESP. A straightforward interpretation of the observations on the basis of a simple band model appears difficult, since the available band structure predict a zero intercept at around 0.3 eV from threshold , in contrast to the observed value of 50 meV.

The plateau between 8 and 9 eV is in agreement with the width of the 3d-band of Ni from X-ray photoemission and the drop to 50 % at high energies suggests that the magnetization at T=273 K. According to the escape depth measurement in Ni, this sheet is 5-10 ^{0}A thick.
These and also some preliminary similar results on (111) surfaces are consistent with the values obtained from polycrystalline films. In these films various surfaces having different work functions are exposed, and the sharp structure at threshold is therefore smeared out .

2.Valence-Band Satellites in Ni:

An instructive example is the use of polarization analysis is the case of the 6eV satellite in Ni metal. This is caused by a two-hole state at the site of one Ni atom , or in other words, it is a state that is

screened by sp-electrons, whereas the main line is due to a hole screened by a d-electron.In the valence band this satellite shows a resonance enhancement at the 3p photothreshold because direct photoemission. At threshold photoabsorption ($\hbar\omega$= 67.7 eV only spin-down (minority) electrons are photoexcited, since only the spin-down band has empty state at the Fermi energy.

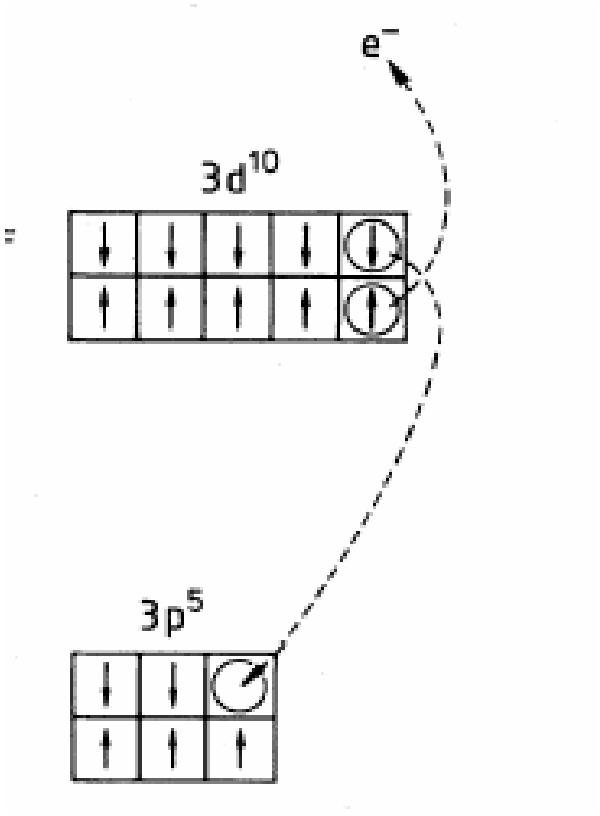

Fig.7 Spin polarization for the 6eV satellite in Ni metal measured at threshold for the photoexcitation of Ni 3p electrons**.**

This results in an intermediate “spin-up” polarized state with a “spin down” hole in the 3p shell. The deexcitation process (Super-coster-Kronig Auger process) which leads to the final $3d^8$ state in the valence band, takes place via the emission of two electrons out of valence band. Since the Auger electrons lead to a singlet (S=0) final state and only spin-down electrons can go into the $3p^5$ state, spin-up electrons must be ejected and positive polarization 60%. Main 3d line corresponds to 3d hole screened by a 3d electron leading to final state $3d^94s$ satellite correspond to to two 3d holes localized on the same site screened by the 4s electrons. Final state $3d^84s^2$ .At 3p there only 3p spin down electron can excite to 3d spin down band because the majority band is occupied.

3. Study of Non-magnetic material:

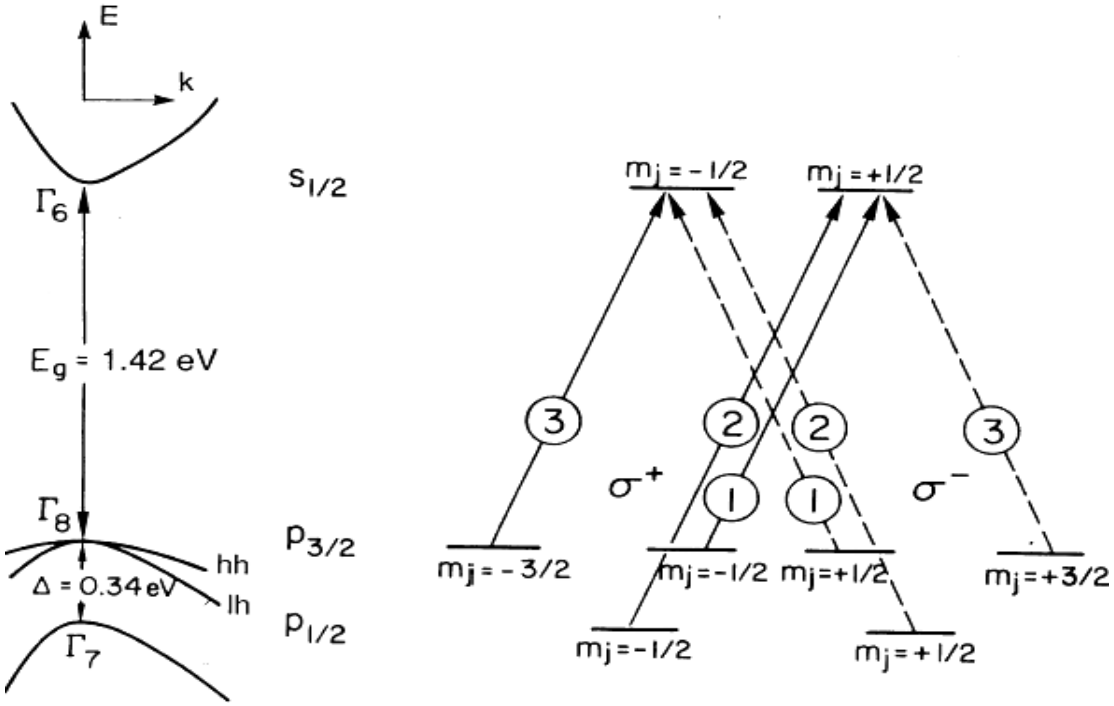

Fig.8 On the left are depicted the energy bands of GaAs at the center of the Brillouin zone showing the band gap energy *E*g and the spin-orbit splitting of the valence band Δ . On the right are shown the allowed transitions between m_j sublevels for circularly polarized light,σ ⁺ (solid lines) and σ ⁻ (dashed lines), with relative transition probabilities given by the circled numbers.

GaAs is a direct-gap semiconductor with the band gap, *E*g, at the center of the Brillouin zone as in the *E*(*k*) plot of the energy bands *vs.* crystal momentum *k* shown on the left side of Fig. 8. The relative intensities for transitions between m_j sublevels by photoexcitation with circularly polarized σ ⁺ and σ ⁻ (positive and negative helicity) light are shown on the right side of Fig. 8. The polarization is defined as $P = (N\uparrow - N\downarrow)/(N\uparrow + N\downarrow)$where $N\uparrow(N\downarrow)$ are the number of electrons with spins parallel (antiparallel) to a quantization direction. Thus, for _+ light, quantum mechanical selection rules give the theoretical polarization, P_{th} = (1–3)/(1+3) = –0.5 for band gap photoexcitation.An important characteristic of the GaAs source is that the sign of the spin polarization of the excited electrons can be easily changed by reversing the helicity of the incident light without affecting other parameters of the electron beam.

3.Surface Studies:

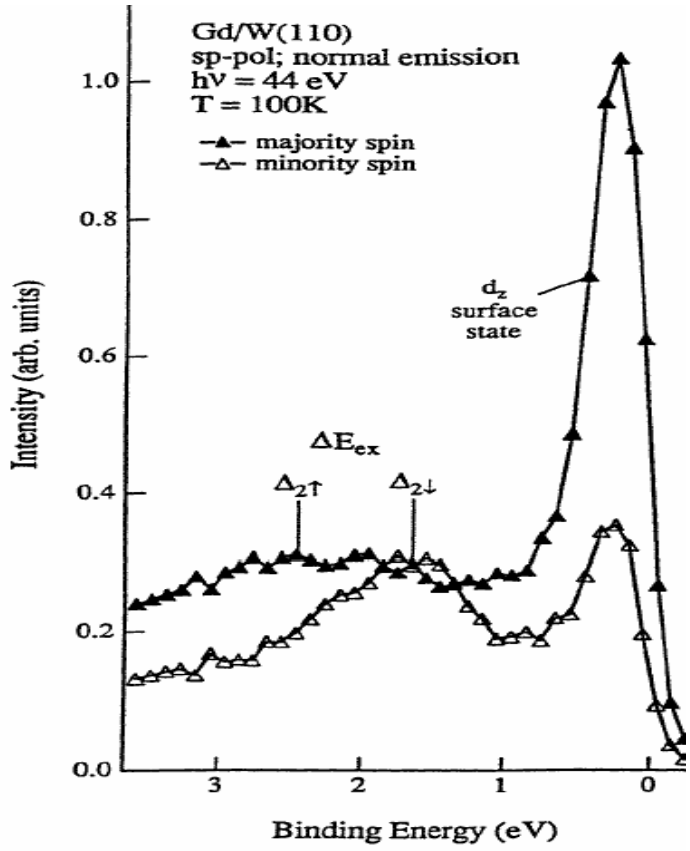

Fig.9 Spin-resolved photoemission spectra recorded along the surface normal from a Gd film grown on a W(110) substrate. The strong majority spin surface state sitting immediately below the Fermi level is clearly visible

Studies have also been carried out on the rare-earth Gd(0001) surface. A spin-integrated photoemission study identified a surface state of dz^2 character 2 eV below the Fermi level . Shown in figure.9, a subsequent spin polarized photoemission study found that this state carried majority spin suggesting that the surface magnetic moments were ferromagnetically aligned with the substrate. Such an observation disagreed both with the results of an earlier spin-polarized photoemission study of the Gd core levels and with a subsequent first-principles total-energy calculation which favoured an antiferromagnetic alignment of the surface and bulk moments. Further spin-polarization studies of the secondary electrons and the Gd 4f core levels confirmed the ferromagnetic alignment but suggested the possibility of a small canting of the surface moments with a component

Thin-film studies

Chromium films deposited on Fe(001) substrates have been extensively studied in thin-film magnetism. The interest stems largely from the oscillatory exchange coupling and giant magneto-resistance that has been observed in the related Fe/Cr multilayers.

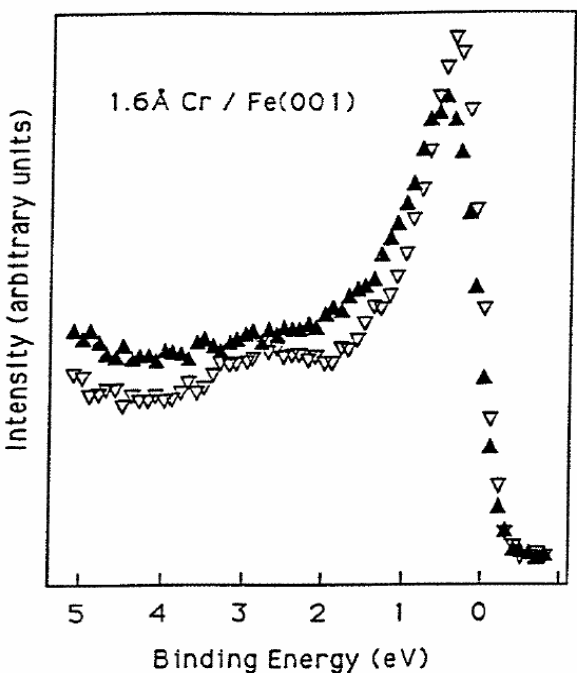

Fig.10 Spin-polarized spectra recorded from approximately one monolayer (1.6 A) Cr deposited on an Fe(001) substrate. The incident photon energy is 52 eV, an energy at which a local minimum occurs in the Fe 3d cross section.

It is measured relative direction of magnetization in an Fe film deposited on a Cr wedge previously deposited on an Fe(001) substrate. The study provided evidence of the oscillatory exchange coupling but also clearly demonstrated the role of interfacial roughness in determining the period length.

Chromium has an identical lattice structure to Fe but its half-filled d-band results in the antiferromagnetic rather than ferromagnetic state representing the lowest energy configuration. In the bulk crystal each atom is antiferromagnetically coupled to its nearest neighbour so that every (001) plane is ferromagnetically aligned within the plane but antiferromagnetically aligned to neighbouring (001) planes. Calculations indicate that a Cr monolayer deposited on an Fe (001) substrate will also be ferromagnetically aligned within the plane but antiferromagnetically aligned to the substrate.The calculations also predict that the moment on the Cr site is considerably enhanced $3.1\mu_B$ as opposed to the $0.6\mu_B$ characteristic of bulk Cr.

There have also been studies of the reverse case, Pd films deposited on Fe substrates. In figure 11 we show an example of spin-polarized interface states observed in a study of Pd deposited on an Fe(110) surface. Pd grows epitaxially on the Fe(110) surface until at a coverage close to one monolayer a phase transition results in the overlayer adopting the (111) structure. Subsequent growth proceeds epitaxially in (111) planes. The study of the Pd(111)/Fe(110) interface, the interface state at a binding energy of 1.5 eV with respect to E_F. The interfacial character was confirmed by its lack of dispersion as the incident photon energy was varied and the observation that its intensity saturated at 1.5 ML.

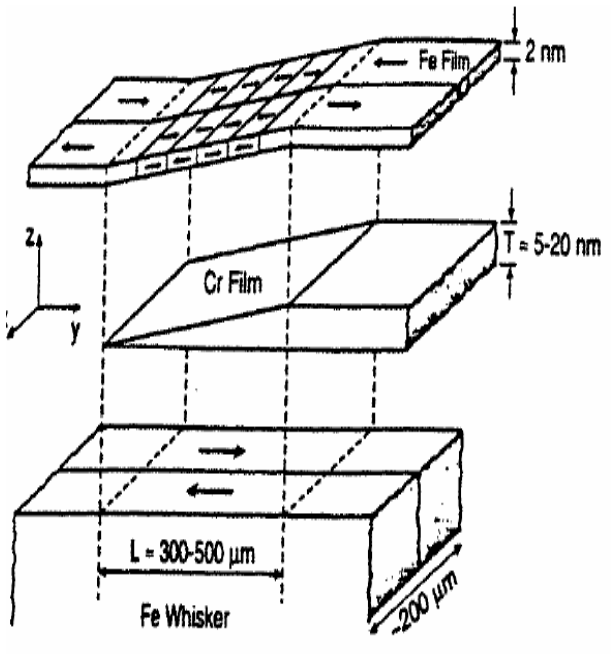

Fig.11 An Fe over layer was deposited on a Cr wedge that had previously been evaporated on an Fe(001) single-crystal whisker. The arrows in the Fe show the direction of magnetization in each domain.

In a separate study of a Pd monolayer deposited on Fe(001), it was again shown that spin-polarized features characterizing the Pd overlayer were evident in the spectra. By examining the spin polarization as a function of coverage, that the polarization of the Pd was confined to the interfacial layer. In fact the spin-polarized spectra indicated that in a 2.1 ML thick Pd film the surface layer had a moment that was already reduced with respect to that characterizing the monolayer. Through comparison with calculation, it was further determined that the magnetization induced in the Pd reflected a strong Pd–Fe interaction rather than a lateral Pd–Pd interaction. Interestingly, a monolayer of Pd on non-magnetic Ag(001) has been predicted to be paramagnetic even though the expansion of the Pd lattice is larger than that associated with Pd on Fe(001). Because of the large exchange splitting in the substrate, it is found that the interaction of the Pd is stronger in the majority spin channel than the minority spin channel. This in turn results in the majority spin states in the overlayer being distributed over a larger range in binding energy than those states of minority spin character. The Fe interface moment for this system was 2.69 μ_B, significantly larger than the bulk value of 2.15 μ_B . A moment of 0.29 μ_B was calculated on the Pd sites for the monolayer coverage.

Summary :

The future prospects of spin polarized photoemission from magnetic material are extremely promising. The potential of the technique for understanding the electronic structure of magnetic metals and alloy has not been exploited and one can expect novel information on surface magnetism and its relation to catalytic phenomena. It is easier to perform spin polarization of non-magnetic material, because one doesn't have to generate a magnetization by external magnetic field and can avoid unfavorable effects.

Application of spin-polarized photoemission has been extensive. Because of its sensitivity to the surface region it has offered a number of new insights into the electronic structure of magnetic surfaces and thin films.

References:

1. Jonson, P. D., *Rep. Prog. Phys*. **1997**, *60***,** 1217.
2. Feuerbacher, B., Fitton, B., Willis, R. F., Photoemission and the electronic properties of surfaces, John Wiley & sons, First Edition, 1978
3. Huang, H., Hermanson H., *J Phys. Rev. B*, **1985**, *32*, 6312.
4. Vescovo, E., *Phys.Rev.B*, **1997,** *56*, 403.
5. Nakajima, N. *et al Phys. Rev.* B **2004,** *70,* 233103.
6. Woods, M., *J. Phys.: Condens. Matter*, **2001**,*13,* 8607.
7. Kessler, J *Chinese J Phys., 1989, 27*, *73.*
8. Clauberg, R. *et al Phys. Rev. Lett.1981,47*, 1314.
9. Eberhardt, W. *et al Phys.Rev.*B **1980**, *21,*3245.